Acta Biomaterialia 198 (2025) 174–187

Contents lists available at ScienceDirect

Acta Biomaterialia

journal homepage: www.elsevier.com/locate/actbio

Full length article

Stretch activated molecule immobilization in disulfide linked double network hydrogels

Yuwan Huang [a], Zihao Li [b], Chavinya D. Ranaweera [b], Pavithra B. Jayathilaka [b], Md Shariful Islam [c], Alaa Ajam [a], Meredith N. Silberstein [d], Kristopher A. Kilian [b,c], Jamie J. Kruzic [a,*]

[a] School of Mechanical and Manufacturing Engineering, University of New South Wales (UNSW Sydney), Sydney, NSW 2052, Australia
[b] School of Chemistry, Australian Centre for NanoMedicine, University of New South Wales (UNSW Sydney), Sydney, NSW 2052, Australia
[c] School of Materials Science and Engineering, University of New South Wales (UNSW Sydney), Sydney, NSW 2052, Australia
[d] Sibley School of Mechanical and Aerospace Engineering, Cornell University, Ithaca, NY, USA

ARTICLE INFO

Keywords:
Polyethylene glycol
Disulfide
Alginate
Double network hydrogels
Mechanical properties
Mechanochemistry
Human fibroblasts

ABSTRACT

Inspired by how forces facilitate molecule immobilization in biological tissues to provide localized functionalization, tough hydrogel networks with stretch activated mechanochemistry are developed by utilizing disulfide bonds as dynamic covalent crosslinks. Specifically, disulfide linked polyethylene glycol hydrogels are reinforced with a second ionically bonded sodium alginate network to simultaneously achieve stretchability and mechanochemical functionalization. To demonstrate and quantify the mechanochemical response, thiols produced by disulfide bond rupture are sensed during stretching using a reaction activated fluorophore dissolved in the hydrating solution. By monitoring the increase in fluorescence intensity upon stretching, it is determined that disulfide bond breakage in the double network hydrogels becomes more activated in hydrogels with high stretchability under low stress. Such results provide guidance regarding how the molecular weights and mass fractions of the monomers must be chosen to design double network hydrogels that balance favorable mechanical properties and mechanochemical responsiveness. Finally, for the most mechanochemically active hydrogel, we demonstrate how the stretch-activated immobilization of a maleimide containing peptide can functionalize the gels to promote the growth of human fibroblasts. Results of this work are anticipated to encourage further research into the development of stretchable and multifunctionalizable hydrogels for biotechnology and biomedical applications.

Statement of significance: Inspired by the mechanochemical dynamics in biological tissues, this work demonstrates the development of hydrogel-based biomaterials that can achieve stretch activated functionalization by molecule immobilization in multiple distinct ways. Using disulfide linked polyethylene glycol hydrogels reinforced with a second alginate network, we have elucidated the structure-property relationships of our hydrogels by functionalizing them with fluorophore to ensure a robust combination of stretchability and mechanochemical responsiveness. We also have demonstrated the capability for using stretch activated immobilization of functional peptides to guide human fibroblasts activity. By demonstrating how hydrogel network properties impact both mechanical and functional performance, this work opens pathways for designing multifunctionalizable hydrogels that adapt to mechanical forces, potentially broadening the application of hydrogels in biotechnology and biomedical applications.

1. Introduction

It has been understood for more than a century that forces exerted on biological tissues stimulate immune response, cellular signalling, matrix synthesis, and tissue remodelling [1,2]. For example, mechanical loading of bone guides matrix deposition and mineralization from osteoblasts [3] while cell generated forces can induce the unwinding of biopolymers to direct specific bioactivities [4]. Accordingly, biological

* Corresponding author.
E-mail address: j.kruzic@unsw.edu.au (J.J. Kruzic).

https://doi.org/10.1016/j.actbio.2025.04.013
Received 19 November 2024; Received in revised form 1 April 2025; Accepted 3 April 2025
Available online 4 April 2025

tissues are dynamic materials where mechanical force can be used to trigger multiple functionalities.

Mechanochemistry in polymers aims to mimic the behavior of biological tissues whereby mechanical stress activates bond scissions and chemical reactions, providing a unique approach to design force responsive smart materials [5–7]. One class of such materials have been developed using disulfide bonds which often act as protein bridges that dynamically break and reform in nature [8]. Motivated by their reversible and dynamic characteristics, disulfide linked hydrogels have recently been developed as potential materials for biomedical engineering applications such as cell culture [9–12], drug delivery [13,14], chemosensors [15], tissue engineering scaffolds [16,17], etc.. Disulfide bonds are relatively more susceptible to breakage compared to other chemical bonds (e.g., dicarbon or carbon-sulfide) and they have been successfully introduced into biocompatible hydrogels as dynamic covalent crosslinks with reversible bond breaking and reforming properties under applied stress [10,18–20]. The selective rupture of the relatively weak disulfide bonds under mechanical force creates free thiols that can further react with their surroundings via thiol-disulfide exchange [18,21,22] or Michael addition [10], demonstrating their potential for stress-responsive applications. Accordingly, disulfide linked hydrogels have recently been developed as dynamic and force responsive materials for potential biomedical applications such as cell culture, drug delivery, tissue engineering scaffolds, etc. [10,19,23–25]. However, previously developed single network (SN) disulfide linked hydrogels are weak and brittle, which is a key limitation for force activated applications, especially when stretching is required under tension loading.

To make hydrogels that are better suited for mechanical loading applications, double network (DN) hydrogels have recently been developed by adding a reinforcing network to improve the mechanical properties [26–28]. It has been established that high stiffness, strength, stretchability, and toughness can be achieved by DN hydrogels [26–28], and there have been some promising advances in the field of mechanochemistry whereby tough and stretchable DN hydrogels have been fabricated where bond scission spontaneously induces a color change [29–33], fluorescence [34,35], molecule release [36,37], or mechanoradical polymerization [38]. A common feature of these previously developed systems is that a single mechanochemical function can be achieved. In contrast, a system where stretch activated immobilization of small molecules solvated in its aqueous environment can be used to functionalize a DN hydrogel in multiple ways has not yet been demonstrated. Furthermore, noting the strong influence of monomer mass fraction and molecular weight on the mechanical properties of DN hydrogels [28], there is a question regarding how to design mechanophore linked DN hydrogels to achieve desirable mechanical strength and stretchability simultaneously with functional mechanochemistry properties.

Accordingly, in the present work we develop tough, stretchable, and mechanochemically active disulfide bonded hydrogels that are reinforced with a second alginate network to create a first demonstration of how stretch activated molecule immobilization can be used to functionalize a DN hydrogel in multiple ways. We first functionalize our DN hydrogels using a fluorophore to determine how the key network variables (i.e., molecular weight and mass fraction) influence the mechanical properties and mechanochemical responsiveness. Finally, we demonstrate stretch-activated immobilization of a maleimide containing peptide to functionalize the gels to promote the growth of human fibroblasts. Results of this work are anticipated to aid the development of stretchable, mechanoresponsive, and multifunctionalizable hydrogels for biomedical applications.

2. Materials and methods

2.1. Materials

All chemicals and reagents were purchased from ChemSupply Australia unless otherwise noted. 5 kDa 4-arm poly(ethylene glycol) thiol (PEG4SH) was supplied by JenKem Technology USA. 10 kDa PEG4SH was provided by JenKem Technology USA and Laysan Bio. Thiol fluorescent probe IV was supplied by Merck (Pty) Ltd Australia.

2.2. Fabrication of double network hydrogels

Double network (DN) hydrogels with compositions in the range of 5–20 wt. % PEG4SH and 1–2 wt. % alginate were achieved by controlling the weight fractions of PEG4SH and sodium alginate powder that were dissolved into deionized water to produce the pregel solutions. To form the covalent hydrogel networks, 33.3 μL of 30 v. % hydrogen peroxide and 20 μL of 0.3 wt. % aqueous sodium iodide solution were added as initiators for each 0.01 mmol of PEG4SH monomer in each pregel solution. The mixture was immediately poured into molds which consisted of two microscope glass slides and a laser-cut silicone sheet to create 1 mm thick custom dog-bone tensile samples with $W = 7.5$ mm gauge width and $L = 3$ mm gauge length as shown in Fig. 1a. After 48 h gelation time in a sealed and moist container at room temperature, the gel samples were taken out of the molds and soaked in 0.1 M $CaCl_2$ solution for around 2 h to crosslink the alginate network. The as-prepared DN gels were kept in a sealed and moist container for further experiments.

2.3. Mechanical characterization of hydrogels

2.3.1. Tensile testing

Tensile tests were performed using a computer-controlled Mark-10 ESM303 mechanical tester with calibrated 100 N and 10 N load cells. At least five specimens for each group were stored in 0.1 M $CaCl_2$ solution overnight to achieve the swollen state. Before testing, the gripping sections of the hydrogel samples were first glued between two polypropylene sheets along one silicone spacer at both ends to avoid damage at the gripping fixtures prior to testing, as shown in Fig. 1b. Then a random speckle pattern was applied to the gauge length region (Fig. 1c) using black spray paint to enable digital image correlation (DIC) determination of the gauge length displacements and strains during the tensile tests [26,39–41]. During testing, glued samples were clamped in wedge grips and were stretched until failure with a displacement rate of 0.5 mm/min and a sampling rate of 2 data points/sec. Videos were recorded during each test for the subsequent DIC analysis and the applied force was simultaneously recorded using MESUR® software. At least five swollen dog-bone tensile samples were tested for each group and in most cases the samples broke within the gauge length. The 5 wt. % 10 kDa PEG4SH + 1 wt. % alginate group was selected for additional tests to understand the effects of strain rate and cyclic loading.

For the rate dependence tests, a higher stretching rate of 5 mm/min with a faster sampling rate of 5 data points/sec was used to test four repeat samples. Cyclic loading tests were performed by stretching two repeat DN hydrogel samples to around 60 % strain at a rate of 0.5 mm/min followed by unloading at the same rate for a total of three loading/unloading cycles. For displacement and strain determination via DIC, images were taken from the recorded videos to match the force record of 2 or 5 data points/sec using a custom MATLAB script. Then, the photos were processed using ZEISS GOM correlate software to measure the deformed gauge length during stretching by tracking the unique speckles within the gauge length in the images. The smoothing tool of

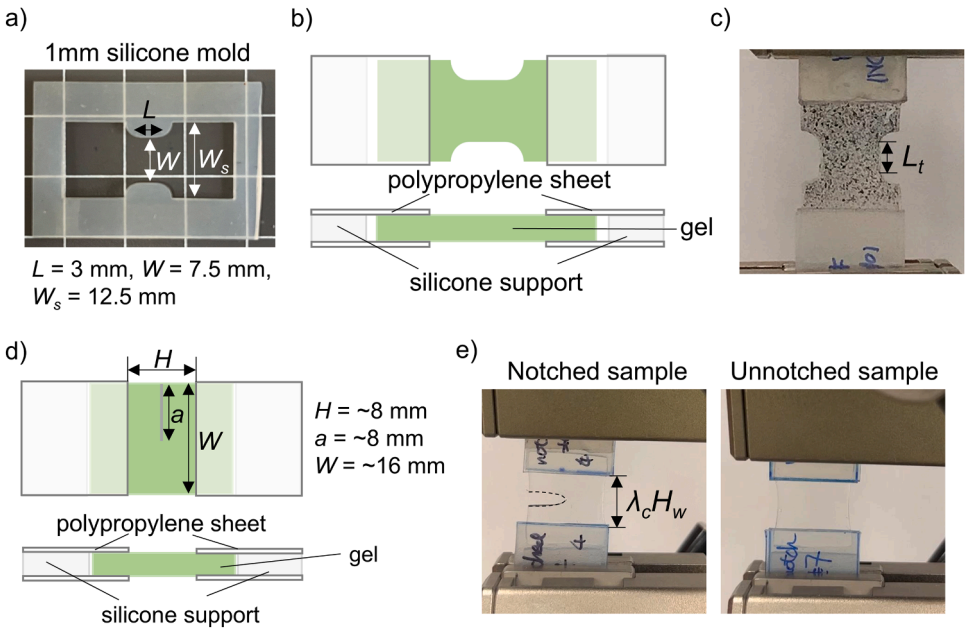

Fig. 1. a) Image of a silicone mold for hydrogel fabrication. b) Schematic of tensile sample preparation. c) A speckle pattern painted on the surface of tensile samples for digital image correlation (DIC) tracking of the deformed gauge length, L_t. d) Schematic of notched sample preparation. e) Images of a notched sample under tension along with the unnotched reference sample.

OriginLab software was used to create smooth load-displacement curves for further analysis.

The engineering strains under tension were calculated from the DIC determined gauge length displacements as $\varepsilon_e = \frac{\Delta L}{L_w}$, where ΔL represents the difference between deformed gauge length, L_t, and original gauge length in the swollen state, L_w. The engineering stresses were calculated as $\sigma_e = \frac{F}{A_w}$, where F was the applied force and A_w was the cross-sectional area of the undeformed wet, swollen gel sample as the product of gauge width, W_w, and thickness, T_w. The tensile modulus of the hydrogels, defined as the ratio of applied change in stress to the strain in the initial region of the engineering stress-strain curve, was determined using the slope of a linear fitting line within the 5–10 % strain region. The work of rupture for each tested sample was calculated as the area under the engineering stress-strain curves up to the failure point.

2.3.2. Fracture toughness testing

Also, for the 5 wt. % 10 kDa PEG4SH + 1 wt. % alginate group additional notched tensile experiments were conducted using the sample configuration shown in Fig. 1d. Rectangular hydrogel sheets with ~1 mm thickness were produced following the previous protocol. After soaking in 0.1 M $CaCl_2$ solution for alginate network forming, the polymerized gel sheets were cut into rectangular samples with about 16 mm × 16 mm × 1 mm size and then stored in 0.1 M $CaCl_2$ solution overnight to achieve the swollen state. Four samples were cut using a razor blade to produce an edge notch with $a \cong$ 8 mm in the middle of stretching area. Before testing, the hydrogel samples were first glued between two polypropylene sheets using silicone spacers similar to the tensile samples. The stretching area had dimensions $W_w \cong$ 16 mm width and $H_w \cong$ 8 mm height as shown in Fig. 1d. A Mark-10 ESM303 mechanical tester with a calibrated 100 N load cell was used to perform the notched tensile tests with a displacement rate of 0.5 mm/min. An unnotched reference sample shown Fig. 1e was also tested until failure to enable calculation of the fracture toughness according to the pure shear test method developed by Rivlin and Thomas [42,43]. For all tests, the applied force and the displacement of the grips was simultaneously recorded using MESUR® software. All samples were tested with the same displacement rate to measure the critical stretch distance, λ_c, where the crack started to propagate and the applied force dropped.

For determination of fracture toughness, nominal stress, σ_e, versus tensile stretch, λ, data was first plotted using the force-displacement data from the unnotched sample. The tensile stretch was determined as $\lambda = \frac{H_w + \Delta H}{H_w}$, where H_w was the original height of the tested sample in the swollen state and ΔH was the displacement recorded from the software. The nominal stress was determined as $\sigma_e = \frac{F}{A_w}$, where F was the applied force and A_w was the undeformed cross-sectional area of the swollen unnotched sample calculated as the product of stretching area width, W_w, and thickness, T_w . The critical stretch, λ_c, for each notched sample was calculated as $\lambda_c = \frac{H_w + \Delta H_c}{H_w}$ using the critical distance, ΔH_c, recorded from software when cracks started to grow during the tests. The fracture toughness of each sample was then calculated as:

$$\Gamma_{fracture} = H_w \int_1^{\lambda_c} \sigma_e d\lambda. \tag{1}$$

2.4. Mechanical modeling

The incompressible Arruda-Boyce model was used to fit the tensile testing data using a custom MATLAB script with a least-squares minimization approach as described previously [13]. Briefly, true stress, σ_t, versus stretch, λ, data were fit with the statistical mechanics-derived form of this model [44,45] as:

$$\sigma_t = \frac{1}{3} n k_b T \frac{N}{\lambda_{ch}} \mathscr{L}^{-1}\left\{\frac{\lambda_{ch}}{\sqrt{N}}\right\}\left(\lambda^2 - \frac{1}{\lambda}\right), \tag{2}$$

where the two material constants "n" and "N" represent the network crosslink density and the number of Kuhn segments between crosslinks, respectively. In this model, the stretch, λ, was defined as $\lambda = 1 + \varepsilon_e$ and the effective chain stretch, λ_{ch}, was defined as $\lambda_{ch} = \frac{1}{\sqrt{3}}\sqrt{\lambda^2 + \frac{2}{\lambda}}$. The true tensile stress σ_t was determined as $\sigma_t = \frac{F}{A_t} = \sigma_e(1 + \varepsilon_e)$ by assuming incompressible deformation. The two material parameters "n" and "N" are helpful to quantitatively describe the effective polymer structure of the hydrogels and to understand how the structure controls the mechanical behavior.

2.5. Mechanochemical testing and image analysis

The measurement of fluorescence intensity induced by mechanochemical reactions is a common method to quantitatively determine the extent of mechanochemical reactions [10,19,29,34,35,46–50]. In this work, to detect the rupture of disulfide bonds, thiol fluorescent probe IV (3-(7-Hydroxy-2-oxo-2H-chromen-3-ylcarbamoyl)acrylic acid methyl ester) was used to react with free thiols to give blue-green fluorescence as illustrated in Fig. 2b [51]. The 3D fluorescence spectra of thiol fluorescent probe IV were measured without and with the presence of thiol. As demonstrated in Fig. 2c, no fluorescence was observed from thiol fluorescent probe IV itself, while strong fluorescence was detected in the presence of 1,2-ethanedithiol in the emission range of 430–470 nm under the excitation wavelength of 290–420 nm. This spectroscopic analysis assisted in the selection of the appropriate filter set used in fluorescence imaging in the following steps.

2.5.1. Mechanochemical testing under tension

For mechanochemical testing, thiol fluorescent probe IV was first dissolved in dimethyl sulfoxide to a concentration of 40 mM and kept in a freezer as a stock solution. Then, 20 v. % fluorescent probe IV stock solution was mixed by gentle shaking with 1 v. % Tween 80 and 79 v. % deionized water to create the dye solution. For mechanochemical tests, 5–20 wt. % 10 kDa PEG4SH with 1–2 wt. % alginate and 5–10 wt. % 5 kDa PEG4SH with 1–2 wt. % alginate DN hydrogels were fabricated as dog-bone tensile samples following the fabrication protocol in Section 2.2. Swollen samples were left in the fume for around 1–2 h to become slightly dehydrated for ease of absorbing the dye solution. Then, 15 μL of dye solution was applied onto each side of the gauge sections of the tensile samples (i.e., 30 μL in total for each sample) and allowed 48 h to permeate the hydrogels as illustrated in Fig. 2d. After dyeing, 0.1 M $CaCl_2$ solution was added to rehydrate the samples to the swollen state. The gripping sections of each dyed sample were prepared as illustrated in Fig. 2d by gluing the samples between two polypropylene sheets at both ends with a silicone spacer. A Deben *in-situ* microtester with a 150

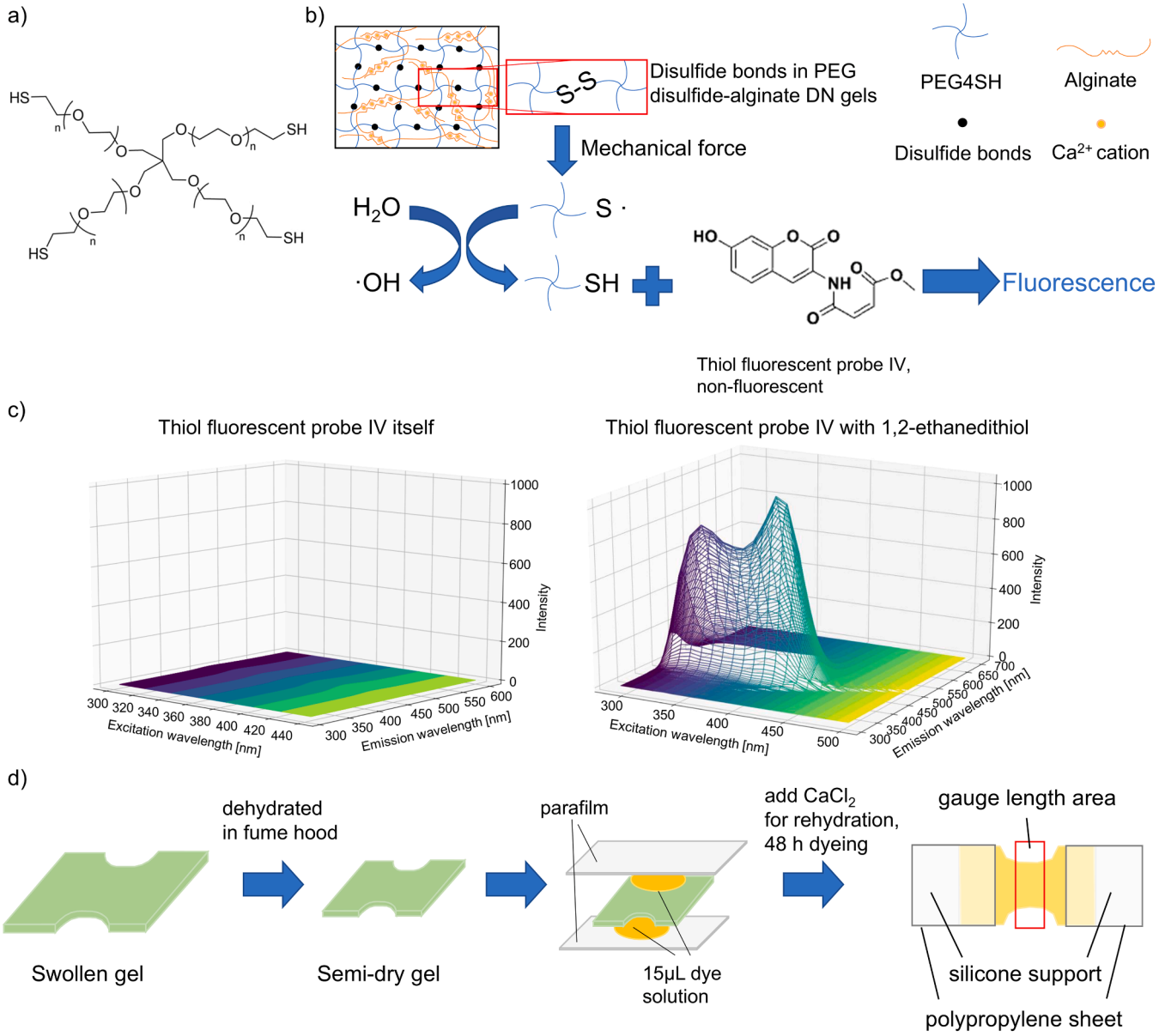

Fig. 2. a) Chemical structure of the PEG4SH monomers. b) Schematics of the mechanochemical reaction between free thiol from broken disulfide bonds in PEG4SH-alginate DN gels and thiol fluorescent probe IV. c) 3D fluorescence spectra of thiol fluorescent probe IV measured without and with thiol from 1,2-ethanedithiol. d) Schematic of the sample dyeing and preparation procedure.

N calibrated load cell was used to stretch the dyed samples at a speed of 0.4 mm/min while observing in a ZEISS Axio Zoom.V16 fluorescence microscope. This was the maximum stretching rate of the Deben *in-situ* microtester, which made testing at 10 times faster stretching rate impossible for these experiments. Hence, a constant strain rate was used for all mechanochemical testing in this work. The microtester was programed to stop and hold at forces equal to the average force corresponding to 0, 15, 30, 45, 60, 75 % of the average measured fracture strain for each group. During each holding point, fluorescence images were recorded in 8-bit grayscale using ZEN software at each measurement strain level with 370–410 nm excitation wavelength using 4 s of exposure time, 100 % light intensity, 7× magnification, and 19.616 μm^2/pixel of spatial scale for each sample. Three dyed samples and one undyed sample as a control sample were tested for each group. For quantitative analysis, ImageJ software was used to analyze the fluorescence images of each hydrogel under the different stretching levels. Since the reacted thiol fluorescent probe IV was excited throughout the thickness of the samples in the region of interest, the mean gray value for fluorescence intensity at a single pixel often decreased due to the decrease in thickness during the test. This motivated us to track the intensity across the entire deformed gauge length to measure the total light emission for a constant volume upon loading. The adjusted integrated fluorescence intensity, I_f, at each tensile strain level after background subtraction was determined in ImageJ as:

$$I_f = A_{\ gauge} \times \left(I_{gauge} - I_{background}\right), \tag{3}$$

where I_{gauge} represents the mean gray value for the entire gauge length and $I_{background}$ was determined by mean gray value of background regions surrounding the gauge length. The background intensities varied sample to sample due to changes in the reflected light from different samples; thus, the background intensity $I_{background}$ was selected as the background region surrounding the gauge length in each image. Then, the fluorescence intensity was plotted as a function of tensile strain and a linear regression fitting was used to determine the slope to represent the mechanochemical reaction sensitivity upon stretching. Intensity values were plotted as mean with standard deviation. The horizontal error bars of intensity represent standard deviation of the actual strains for three tested samples at each force holding point, while the vertical error bars represent standard deviation of adjusted integrated fluorescence intensity values from three tested samples at each imaging point.

2.5.2. Cyclic and notched mechanochemical testing

In addition, the 5 wt. % 10 kDa PEG4SH + 1 wt. % alginate group was also used for cyclic fluorescence tests with the same setup. For these longer tests, 25 μL 0.1 M $CaCl_2$ solution was applied onto the surface at the beginning of each test to reduce drying during the testing. Three dyed hydrogel samples were pulled to 0, 15, 30, 45, 60 % of the average measured fracture strain at the speed of 0.4 mm/min and then were unloaded for a total of two loading/unloading cycles. The mechanochemical response was recorded and analyzed as a function of strain for both loading and unloading as described above. To calculate the linear regressions of intensity versus strain, the engineering strains during the loading processes were determined as $\varepsilon_e = \frac{L-L_w}{L_w}$, where L represents the deformed gauge length and L_w the original swollen gauge length. In contrast, the strains during unloading were calculated as engineering strain under compression starting from the maximum deformed gauge length. I.e., calculated as $\varepsilon_e^{unload} = \frac{L_{max}-L}{L_{max}}$, where L_{max} represents the maximum deformed gauge length during the previous tensile loading cycle.

Finally, the energy dissipation at notch tips has been observed to induce strong mechanochemical reactions [34,35,49]. To observe the intense mechanochemical reaction at the high strains associated with a notch tip, the 5 wt. % 10 kDa PEG4SH + 1 wt. % alginate group was used to perform notched tensile tests in the presence of the thiol fluorescent probe IV dye solution using the same sample configuration shown in Fig. 1e. After 1 hour dehydration in a fume hood, 30 μL of dye solution was applied onto the rectangular 16 mm × 16 mm × 1 mm samples following the previously described protocol allowing 48 h for the dye solution to permeate the hydrogels. Next, 0.1 M $CaCl_2$ solution was added to rehydrate the samples to the swollen state. Before testing, the hydrogel samples were first glued between two polypropylene sheets along one silicone spacer for a stretching area with $W_w \cong 16$ mm width and $H_w \cong 8$ mm height (Fig. 1e). An edge notch with $a \cong 8$ mm length was cut at the middle of stretching area using a razor blade after dyeing and swelling, and before testing. Two dyed hydrogel samples were pulled to 0, 20, 40, 60, 80 % of the average measured critical stretch, λ_c, at the beginning of crack propagation at the speed of 0.4 mm/min. Images were taken in 8-bit grayscale using ZEN software at each measurement strain level under the same excitation wavelength using 4 s of exposure time, 100 % light intensity, 12.5× magnification, and 6.150 μm^2/pixel of spatial scale for each sample. To visualize the mechanochemical response at crack tip, images were converted into a matrix with pixel values and then plotted as contour maps in OriginLab software with a 0–255 color scale range representing the measured fluorescence intensity for 8-bit images. In addition, pixel values along a line passing the crack tip in the crack propagation direction from the images of 20–60 % of critical stretch was exported using ImageJ and then smoothed using Lowess method in OriginLab for line plots of fluorescence intensity to further characterize the damage zone around each crack tip.

2.6. Cell experiments using stretch functionalized samples

2.6.1. Synthesis of thiol reactive Mal-GRGDS peptide

Initially, the Gly-Arg-Gly-Asp-Ser (GRGDS) peptide sequence was synthesized via standard Fmoc solid-phase peptide synthesis on a 2-chlorotrityl chloride resin using benzotriazol-1-yloxytripyrrolidinophosphonium hexafluorophosphate (PyBOP, 0.25 M) and N,N-diisopropylethylamine (DIPEA) as coupling agents. All amino acid coupling steps were performed on a Biotage® Initiator+ Alstra™ automated microwave peptide synthesizer. Upon coupling of the final amino acid, the terminal Fmoc group was removed using 20 % (v/v) piperidine in N,N-dimethylformamide (DMF) for 20 min and manually functionalized with a terminal maleimide group on resin (Fig. 3), using a method adapted from Borsenberger et al. [52]. Briefly, a solution of 3-maleimidopropionic acid (4 equiv.), hydroxybenzotriazole (HOBt)/hexafluorophosphate benzotriazole tetramethyl uronium (HBTU, 4 equiv.) and DIPEA (5 equiv.) in dichloromethane/N, N-dimethylformamide (1:1, v/v) was added to the resin and allowed to shake overnight. Upon confirmation of the coupling using the Kaiser Test, the functionalized Mal-GRGDS peptide was cleaved using a 95 % trifluoroacetic acid, 2.5 % triisopropylsilane, and 2.5 % water (v/v) cleavage cocktail for a minimum of 2 h. The cleavage solution was precipitated in cold ether yielding an off-white precipitate that was concentrated via centrifugation. The ether was then decanted, and the pellet was dried in air. The crude peptide was then purified using a semipreparative high-performance liquid chromatography system equipped with a 254 nm and 210 nm UV detector and characterized using liquid chromatography-mass spectrometry.

2.6.2. Cell culture and immunofluorescence analysis

For cell culture experiments, the 5 wt. % 10 kDa PEG4SH + 1 wt. % alginate hydrogels were fabricated as dog-bone tensile samples following the fabrication protocol described in Section 2.2 and then stored in 0.1 M $CaCl_2$ solution overnight the achieve the swollen state before testing. After preparation of the gripping sections (Fig. 1c), three samples were stretched to 75 % of the average measured fracture strain at a speed of 0.4 mm/min using the same Deben *in-situ* micro-tester with a 150 N calibrated load cell. The synthesized Mal-GRGDS peptide was first dissolved in Milli-Q water for a final concentration of 8 mM, 30 μL

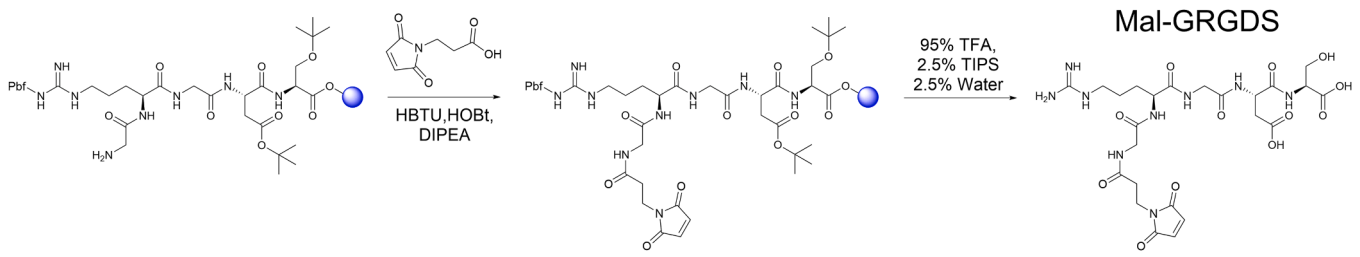

Fig. 3. Synthesis reaction of the Mal-GRGDS peptide used in this study.

of which was added on the surface of stretched samples with 1 min of holding time before unloading. Three samples without stretching were also coated with 30 μL peptide solution as the control group. In both cases, the peptide was then allowed to react for 1 hour before the gels were washed thrice with Milli-Q water.

Human fibroblast (HFF-1) cells were purchased from the American Type Culture Collection (ATCC, SCRC-1041) and cultured in high glucose Dulbecco's Modified Eagle Medium (DMEM) supplemented with 10 % fetal bovine serum and 1 % penicillin/streptomycin. The cells were passaged at approximately 80 % confluency, maintained at 37 °C and 5 % carbon dioxide, and used at passage 22. Prior to cell seeding, the washed and functionalized hydrogels were sterilized under UV for 30 min and washed again with sterile phosphate buffered saline (PBS). Cells were seeded onto the gel surface with an approximate area of 40 mm^2 at a density of 3×10^4 cm^{-2} and allowed to adhere for 1 hour at 37 °C before the slow addition of media.

Cells were cultured on the hydrogel matrices for 48 h before fixing with 4 % paraformaldehyde at room temperature for 30 min. The gels were washed with PBS no more than three times, then cells were permeabilized with 0.5 wt. % Triton-X 100 in PBS for 30 min and blocking was performed using 1 % bovine serum albumin (BSA) in PBS (w/v) for 15 min. Antibody solutions were made using 4′,6-diamidino-2-phenylindole (DAPI, 1:500) and 488 Phalloidin (1:500) in 1 % BSA in PBS (w/v). The staining solutions were added to fixed samples and incubated at room temperature for 1.5 h before washing with PBS no more than three times.

All immunofluorescence images were taken on a ZEISS LSM 900 upright confocal microscope and acquired using a 10×/0.45 or 20×/0.8 objective. All images were analyzed using FIJI (Fiji is Just ImageJ) software.

2.7. Statistical analyses

Tensile and mechanochemical test results were determined from repeat samples as mean ± standard deviation (SD). Since Levene's tests for the swelling properties and tensile test results indicated non-equal variances among many groups, the Kruskal-Wallis test followed by Dunn's post-hoc testing was performed to determine the effect of each individual variable on swelling ratio and stretch along with the tensile modulus, strength, strain to failure, and work of rupture. Additionally, the effect of mass fraction of PEG4SH on swelling and mechanical properties was examined for each combination of molecular weight of PEG4SH and mass fraction of alginate using a linear regression analysis. For the comparison of displacement loading rates for the 5 wt. % 10 kDa PEG4SH + 1 wt. % alginate group, the variances were equal and results were compared using an independent-samples *t*-test.

For the mechanochemical results under tension, the slopes of the adjusted integrated intensity versus strain were determined for each sample. Levene's test indicated equal variances for the mean values, so a three-way analysis of variance (ANOVA) was used with molecular weight, mass fraction of PEG4SH, and mass fraction of alginate as the three independent factors. Additionally, cyclic loading mechanochemical tests were only conducted for the 5 wt. % 10 kDa PEG4SH + 1 wt. % alginate group, so independent samples *t*-tests were conducted to compare the slopes to previously tested single loading samples. All statistical tests for mechanical and mechanochemical testing were performed using IBM SPSS software and a *p*-value smaller than 0.05 was considered statistically significant. As for cell experiment results, unpaired *t*-tests with Welch's correction were conducted in GraphPad Prism.

3. Results and discussion

3.1. Mechanical response under tension

After sample fabrication, the tensile samples were immersed in 0.1 M $CaCl_2$ solution overnight. In general, the amount of swelling was small for all groups and there was a slight trend of more swelling for higher mass fractions of PEG4SH and lower mass fractions of alginate in the double networks (Figure S1, Supporting Information). For DN gels with higher mass fractions of PEG4SH, denser networks with less initial water in the interpenetrating network structures were formed during the fabrication process. Such structures with less initial water mass had a higher capacity for water uptake and were less affected by the alginate additions to resist swelling. This trend matches the reported swelling properties for other PEG-based DN hydrogels [28] while noting that the range of values for the swelling properties across the groups was small, with a range of 0.1–0.3 g/g for the swelling ratio and 1–1.15 for the swelling stretch.

Average tensile modulus, fracture stress, fracture strain, and work of rupture values determined from the engineering stress-strain curves are summarized in Figs. 4a-d. Parameters obtained from fitting the tensile data to the Arruda-Boyce model [44,45] are given in Table S1 (Supporting Information) and statistical test results are given in Tables S2–S6 (Supporting Information). For most groups, a minimum of three specimens of the five tested samples failed within the gauge length as expected (Fig. 4e) and the average results presented in Fig. 4 excluded any gripping point failures. The exceptions were the 5 wt. % 5 kDa PEG4SH + 2 wt. % alginate group and both 5 wt. % 10 kDa PEG4SH double network groups. For those three groups, all tested specimens failed near their gripping points after stretching significantly more prior to failure compared to the other groups (Fig. 4e). The modulus values in Fig. 4a were measured during the first 5–10 % of strain and were thus unaffected by the different modes of failure. In contrast, the measured fracture stress, fracture strain, and work of rupture values for those three groups are considered lower bound estimates due to the premature failure and those lower bound groups are marked with red boxes in Figs. 4b–d.

Increased mass fraction of alginate from 1 to 2 wt. % generally created stiffer, stronger, and tougher double network hydrogels regardless of mass fraction and molecular weight of the PEG4SH monomers as shown in Figs. 4a-d. The increase in modulus and strength resulted from the added alginate network supporting some of the applied stress and thus imparting more stiffness and delaying fracture of the whole system to give higher strength and work of rupture. This reinforcement effect of alginate was more significant for the hydrogels with lower mass fraction of PEG4SH. Indeed, the higher modulus was statistically significant ($p < 0.05$) for the 5 wt. % groups and the higher

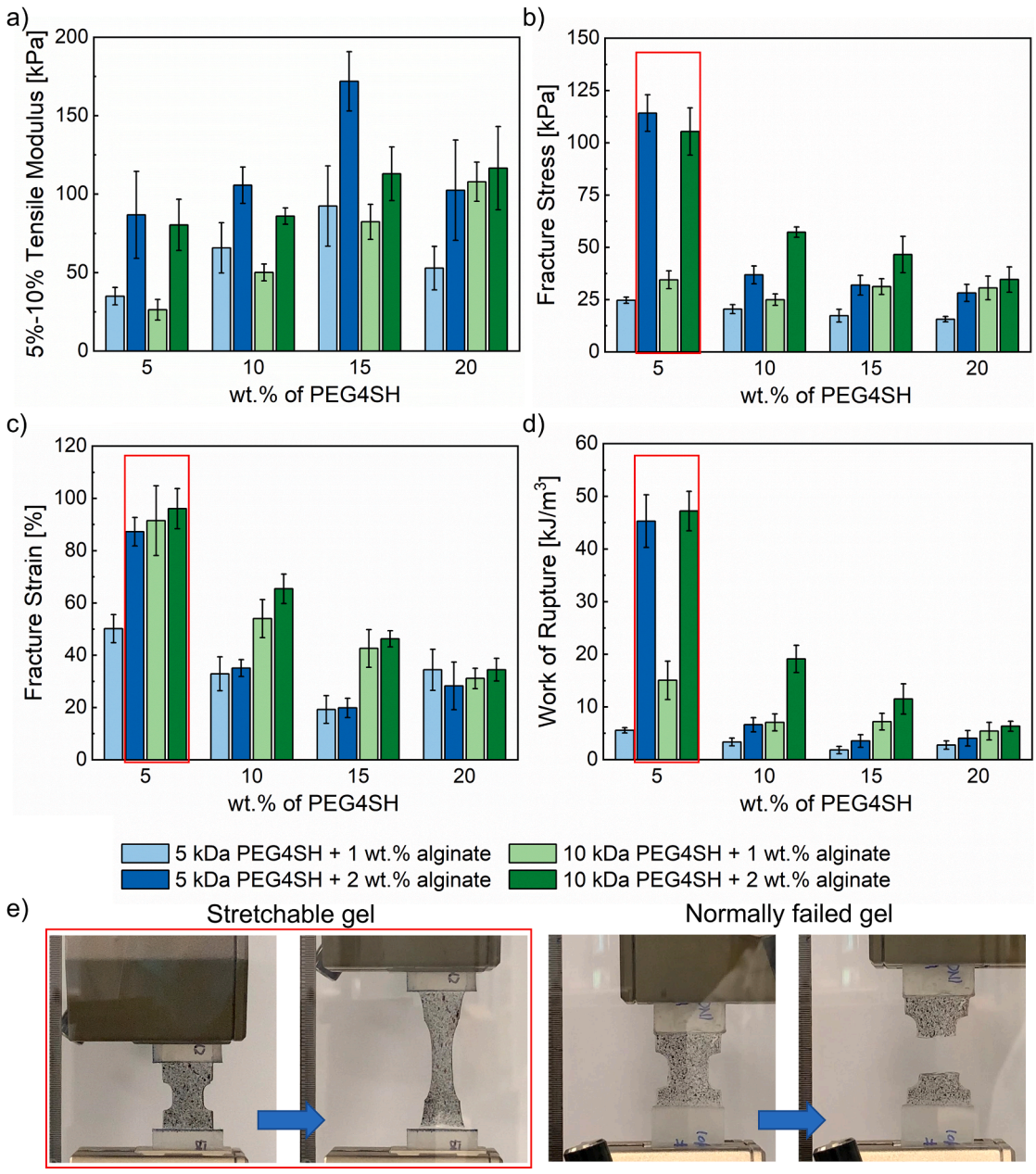

Fig. 4. Mechanical characterization results as mean values with error bars showing the standard deviations for the PEG disulfide-alginate DN hydrogels under tension: a) tensile modulus within 5–10 % strain, b) fracture stress, c) fracture strain, and d) work of rupture. Values in red rectangles in b–d are considered lower bound estimates because they failed prematurely at the gripping point. e) shows at left a highly stretchable 5 wt. % 10 kDa PEG4SH + 2 wt. % alginate sample just prior to failure occurring near the gripping point while at right shows a typical gauge length failure for a 10 wt. % 10 kDa PEG4SH + 1 wt. % alginate sample.

tensile strength was statistically significant ($p < 0.05$) for both the 5 wt. % and 10 wt. % groups (Table S2, Supporting Information). Fitting the data to the Arruda-Boyce model [44,45] indicated that this is due to higher effective network crosslinking density, n, values for the 2 wt. % alginate groups compared to the 1 wt. % alginate groups (Table S1, Supporting Information). It is important to recognize that for double network gels that the model variables n and N represent effective network parameters related to the overall hybrid DN structure rather than directly representing the PEG4SH or alginate chains individually. However, as with our previous work, we find the Arruda-Boyce fit parameters are helpful for interpreting the trends in mechanical properties with changes in the network characteristics [28]. With a relatively low concentration of 5 wt. % PEG4SH, the benefit of alginate reinforcement to the load-bearing capacity of the DN hydrogels was greatest with the stiffness and tensile strength tripling with double the concentration of alginate (Figs. 4a–b). For those cases, the looser covalent PEG4SH network, indicated by the larger effective number of Kuhn segments, N, between crosslinks (Table S1, Supporting Information), is thought to create more open volume for alginate interpenetration, crosslinking, and stretching upon loading. In contrast, there was no statistically significant effect ($p > 0.05$) on the fracture strain for any groups when increasing from 1 to 2 wt. % alginate (Table S2, Supporting Information).

When considering the effect of PEG4SH, higher mass fraction gave higher stiffness but lower fracture stress, fracture strain, and work of rupture. These trends were confirmed by linear regression models that showed statistically significant correlations between mass fraction of PEG4SH and the mechanical properties for most cases when the other variables were held constant (Table S6, Supporting Information). Moreover, increasing molecular weight of the PEG4SH from 5 to 10 kDa led to lower swelling (Figure S1, Supporting Information) and modulus

and higher strain to failure, strength, and work of rupture (Fig. 4). However, the Kruskal-Wallis tests indicated that these differences were rarely statistically significant (Table S5, Supporting Information). Overall, such results are similar to what was found for alginate reinforced PEG (meth)acrylate DN hydrogels [28].

The 5 wt. % 10 kDa PEG4SH + 1 wt. % alginate group was chosen to evaluate the strain rate sensitivity of the mechanical properties due to its high stretchability (Fig. 4c) and promising mechanochemical response that will be described below. Testing at a higher displacement rate of 5 mm/min produced similar moduli and strains to failure (Table S7, Supporting Information) suggesting strain rate insensitive behavior over this range of displacement rates that was considered practical for stretch activated functionalization by molecule immobilization. The low strain rate sensitivity found over this displacement rate range is in agreement with other PEG-alginate DN hydrogels [28,53], although future work may wish to examine a wider range of strain rates, e.g., by rheometry or dynamic mechanical analysis.

3.2. Mechanochemical response under tension

Tensile test results (Fig. 4) highlighted that the work of rupture and stretchability of PEG4SH-alginate DN hydrogels varied considerably for different combinations of molecular weight and mass fraction. In all cases, a higher mass fraction of alginate led to increases in stiffness, strength, and work of rupture as the alginate network was able to support a higher level of stress. This reinforcement effect in turn reduces the available stress on the PEG4SH network to break disulfide bonds and thus induce a mechanochemical reaction. To understand the effects of the network characteristics on the mechanochemical responsiveness, most groups were evaluated except for the least stretchable and lowest work of rupture groups with PEG4SH molecular weight of 5 kDa and mass fractions of 15–20 wt. %. As described in Section 2.5, all tensile samples for the mechanochemical tests were fabricated from pregel solutions in custom silicone molds with 7.5 mm gauge width and 3 mm gauge length and dyed using a thiol fluorescent probe IV fluorophore solution. The reaction rate of this molecule with thiols has been reported to be on the order of 0.01 s [51]; thus, by monitoring the fluorescence intensity of hydrogels during stretching in the presence of solvated thiol fluorescent probe IV, we get a measure of the relative amount of S-S cleavage with different amounts of stretching as well as a direct measure of the capacity of those broken bonds for small molecule immobilization.

Fig. 5a shows the visible fluorescence difference before (undyed) and after (dyed) the hydrogels were saturated with a dye solution containing thiol fluorescent probe IV fluorophore even before mechanical testing. The results in Fig. 5a indicate that the thiol fluorescent probe IV fluorophore in the dye solution reacted with free thiols to some extent prior to stretching. For each group, three samples were designed to be stretched from 0 to 75 % of the expected fracture strain under a fluorescence microscope using an *in-situ* microtester with the thiol fluorescent probe IV fluorophore solution soaked into the swollen samples. However, some tested samples failed prior to producing data for 60 and 75 % of the fracture strain either because they hit the travel limit of the *in-situ* microtester or they experienced unexpected fracture at a gripping point. In the latter case, this may have been a weakening effect of the dye where thiols that reacted with the dye molecules were disabled from reacting with other thiols to dynamically form new disulfide bonds in a self-healing manner. Nonetheless, the results presented in Figs. 5b–d include a minimum of four strain levels (i.e., 0, 15, 30, 45 % of expected fracture strain) for all groups.

The adjusted integrated intensity in each image taken at each measurement strain level with 370–410 nm excitation wavelength was determined over the entire gauge length area after background subtraction (see Section 2.5) and is plotted as a function of the tensile strain

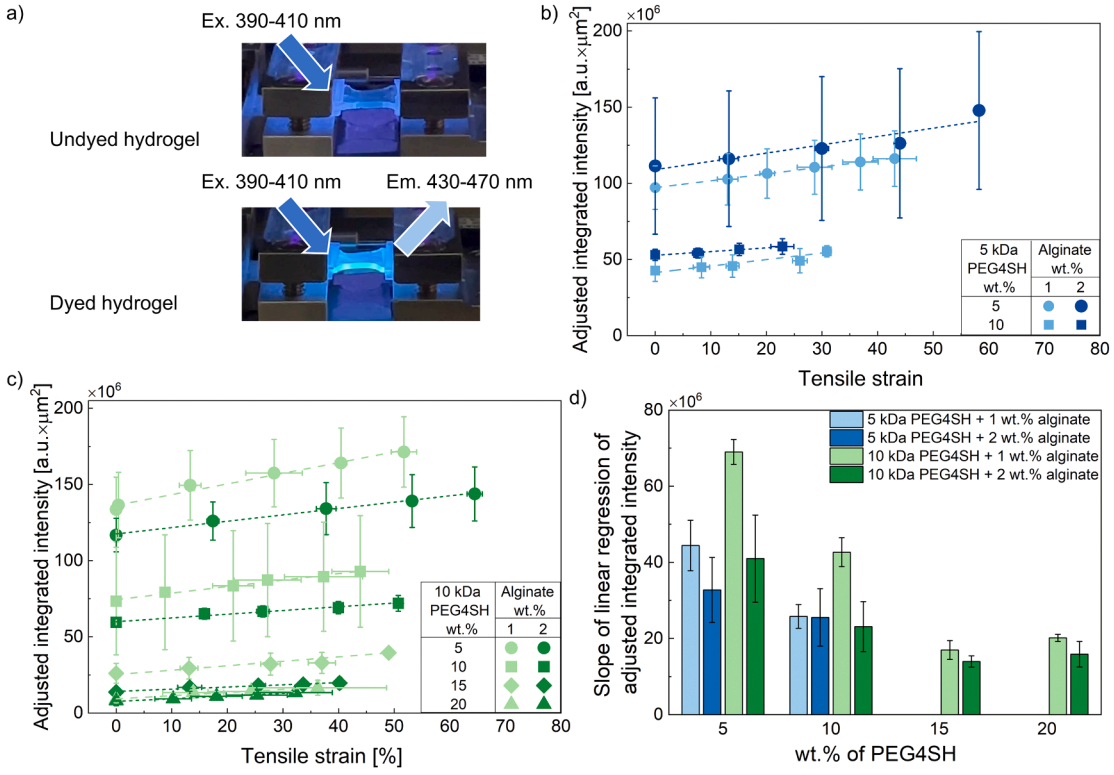

Fig. 5. a) Images of undyed and dyed hydrogels under the excitation of the fluorescence microscope. The adjusted integrated intensity plotted versus engineering strain for b) 5 kDa PEG4SH DN gels (blue) and c) 10 kDa PEG4SH DN gels (green), in which the horizontal error bars represent standard deviation of the actual hold strains during fluorescence data collection and the vertical error bars represent standard deviation of adjusted integrated intensity from three tested samples at each measurement point. d) Summary of the slopes of the linear fitting lines for adjusted integrated intensity versus engineering strain for each tested group.

level in Figs. 5b–c. It can be seen from Figs. 5b–c that the various PEG4SH-alginate DN gels have different baseline intensities before the tests, and the groups with the lowest mass fraction of 5 wt. % PEG4SH had the largest initial total intensity. To quantify the change of fluorescence intensity upon stretching, linear regression analysis was applied for each group. For most groups the coefficient of determination (R^2) values of the fitted trendline functions were higher than 0.9; hence, the linear regression slope of adjusted integrated intensity versus strain was used to represent the sensitivity of the mechanochemical response and the average slope values are summarized in Fig. 5d. The slope values in Fig. 5d represent the incremental increase in fluorescence intensity with stretching relative to the baseline value for each sample type. While the slopes of undyed control samples revealed constant total intensity (Figure S2, Supporting Information), the positive slopes of dyed samples in Fig. 5d quantitatively showed that the total intensity for all tested groups increased upon stretching, indicating the mechanochemical reaction between the fluorophore molecules and the free thiols generated from broken disulfide bonds. Increased mass fraction of alginate from 1 to 2 wt. % gave a smaller slope of intensity change for the same covalent PEG4SH network. In addition, higher mass fraction and smaller molecular weight of PEG4SH monomers also resulted in smaller slopes for fluorescence intensity change. The three-way ANOVA results (Table S8, Supporting Information) indicated that all three factors (PEG4SH molecular weight, wt. % PEG4SH, and wt. % alginate) had statistically significant effects with p values smaller than 0.01.

While alginate reinforcement provides the DN hydrogels with enhanced mechanical properties, a lower mechanochemical reaction activation with straining was found with increasing mass fraction of alginate regardless of the mass fraction and molecular weight of PEG4SH (Fig. 5d). This result is attributed to the alginate network shielding the PEG disulfide network from the applied stress by creating a higher effective crosslink density, as indicated by the higher n values from the Arruda-Boyce model (Table S1, Supporting Information). The decrease in mechanochemical activity also corresponded to higher strength and stiffness, as seen in Figs. 4a–b. Thus, there is a need to balance the mechanical properties with the mechanochemical responsiveness, and a combination of low strength and stiffness and high stretchability resulted in the best mechanochemical performance for the 5 wt. % 10 kDa PEG4SH + 1 wt. % alginate group. Furthermore, while a minimum amount of alginate is required to achieve the high stretchability, too much alginate mainly strengthens and stiffens the DN hydrogel at the expense of both stretchability and mechanochemical response. Such results suggest that the disulfide bond breakage mechanism occurs most efficiently for DN hydrogels that achieve relatively high strain at low stress.

Prior to the mechanochemical testing, all samples dyed with the thiol fluorescent probe IV solution had non-zero initial fluorescence intensity that decreased with increasing mass fraction of PEG4SH (Figs. 5b–c). Samples with higher concentration of PEG4SH had larger initial as-prepared gauge section areas caused by differences in the alginate network formation before overnight swelling (Figure S1, Supporting Information). Thus, despite having a larger sample gauge section area for collecting the fluorescence signal, samples with more PEG4SH showed lower initial intensity. The non-zero initial intensity occurred due to reactions with some of the free thiols initially present in the DN hydrogels. These free thiols may exist because they never formed a disulfide bond during free radical polymerization or because disulfide bonds broke due to swelling stretch, as has been reported for polyacrylamide hydrogels with weak disulfide links [24]. Trends in the initial intensity integrated over the gauge area (Fig. 5) did not correspond to the trends in swelling (Figure S1, Supporting Information); therefore, the lower initial fluorescence intensity with higher PEG4SH concentration was attributed to fewer unreacted thiols and more complete polymerization before adding the thiol fluorescent probe IV dye solution. In contrast, lower mass fractions of PEG4SH monomers gave both a higher baseline intensity along with larger variability for those groups (i.e., larger error bar in Figs. 5b–c) due the relatively poorer and inhomogeneous polymerization that occurred.

The mass fraction of PEG4SH also had a significant impact on the mechanochemical response for the DN hydrogels (Fig. 5d). When PEG4SH molecular weight and alginate concentration were kept constant, a higher mass fraction of PEG4SH generally gave a smaller fluorescence intensity change with strain as indicated by the smaller slopes of the linear regressions shown in Fig. 5d. As mentioned previously, disulfide bond breakage appears to be more activated for DN hydrogels that achieve relatively high strain at low stress. Thus, since the DN hydrogels with more PEG4SH are stiffer, they exhibit less strain per unit of stress and thus less mechanochemical reaction. Indeed, the best performing groups in Fig. 5d also tended to have the lowest elastic moduli in Fig. 4a. In this regard, the stretchable DN hydrogels behave somewhat like unreinforced, single network PEG4SH hydrogels in compression where the highest mechanochemical reaction activation is found for hydrogels formed by the smallest mass fraction of PEG4SH with the lowest elastic moduli [19].

Relatively lower initial fluorescence intensity and a smaller slope for the reaction activation were observed for the 5 kDa groups compared to 10 kDa with other variables held constant (Fig. 5). Regarding the initial intensity, a shorter monomer arm length appears to decrease the likelihood of leaving unreacted thiols in the network after polymerization. Similarly, the shorter effective chain lengths in the final network (i.e., smaller N values in Table S1, Supporting Information) provide higher stiffness that more effectively resists deformation of the whole structure and delays disulfide bond breakage, which may be attributed to a network with a higher degree of structural order with fewer dangling thiols creating weak spots.

3.3. *Mechanical and mechanochemical response under cyclic loading conditions*

Representative tensile results for 5 wt. % 10 kDa PEG4SH + 1 wt. % alginate samples cyclically loaded and unloaded three times are plotted in Fig. 6a. The first loading curve was relatively more linear than the second and third, and the largest energy dissipation of around 3.74 kJ/m^3 occurred during the first loading-unloading cycle. After the initial "shake-down" cycle, the mechanical performance of the DN hydrogel demonstrated a similar nonlinear loading/unloading behavior and smaller energy dissipation (1.39 and 1.13 kJ/m^3) for the following two cycles. In addition, 5 wt. % 10 kDa PEG4SH + 1 wt. % alginate gels were also used to investigate mechanochemical response during cyclic loading since they demonstrated the largest fluorescence intensity change in the monotonic tensile tests. Results for a representative sample showing the adjusted integrated intensity change over two loading/unloading cycles are presented in Fig. 6b and the mean slopes from three tested samples are summarized in Fig. 6c. The largest slope was obtained for the first loading where the most significant amount of disulfide bond rupture is expected. An independent-samples t-test indicated the data from the first loading in the cyclic test was not significantly different from the previous results for 5 wt. % 10 kDa PEG4SH + 1 wt. % alginate group shown in Fig. 5d ($p > 0.05$). It is also worth noting that the total intensity over the gauge length area kept increasing during the first unloading and that the second loading had a decreased slope compared to the first loading. The total intensity then became constant during the second unloading as shown in Fig. 6b for one representative sample and as summarized as a slope close to 0 as shown in Fig. 6c for the three repeat samples.

During cyclic loading, all three unloading curves and the second and third loading curves were found to closely overlap for all samples (Fig. 6a) indicating a short "shake-down" period to reach a nearly steady state behavior, as has been reported for other alginate reinforced hydrogels [54,55]. Some previous studies have attributed the "shake-down" cycle to alginate chains unzipping at large deformations because the corresponding unreinforced single covalent network hydrogels

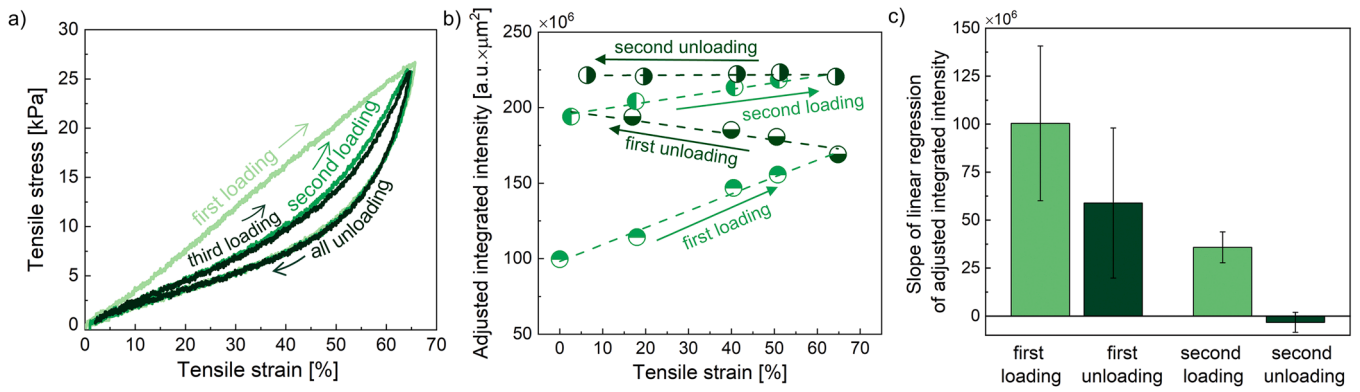

Fig. 6. Representative a) cyclic engineering stress-strain hysteresis curves and b) adjusted integrated intensity data for a cyclic mechanochemical test of one sample in the 5 wt. % 10 kDa PEG4SH + 1 wt. % alginate group. c) Mean slopes with error bars showing the standard deviations for the adjusted integrated intensity versus engineering strain based on three repeat samples. For the unloading curves, the slope was determined from the engineering strain under compression starting from the maximum deformed gauge length as described in Section 2.5.2.

exhibit little hysteresis during cyclic loading [15,26–28,40]. However, in the present study the relatively weak and dynamic disulfide bonds also contribute to the energy dissipation. Indeed, mechanochemical testing with the thiol fluorescent probe IV solution revealed increasing fluorescence intensity with strain (Fig. 5) indicating the cleavage of disulfide bonds upon stretching. Interestingly, the integrated intensity kept increasing during the first unloading in Fig. 6b, showing that ruptured disulfide bonds continue reacting with the local chemical environment during force releasing. Here, the increasing intensity with each increment of strain release may be associated with the extent of molecular motion promoted by each unloading step. During the second loading there was a further increase in fluorescence intensity which can be explained by two potential mechanisms that likely acted together. For one mechanism, unreacted thiols generated during the first loading may have continued to react with the local chemical environment during the second loading in a similar manner to the first unloading process. Additionally, there may have been some generation of new thiols during the second loading due to the redistribution of stresses in the network from disulfide bonds breaking during the first cycle. Finally, for the second unloading no further reaction occurred in the PEG4SH network as the intensity remained constant (Fig. 6c). The saturation of the mechanochemical reaction after the second loading agreed well with the cyclic mechanical performance where the hysteresis loop stabilized in Fig. 6a after the second loading.

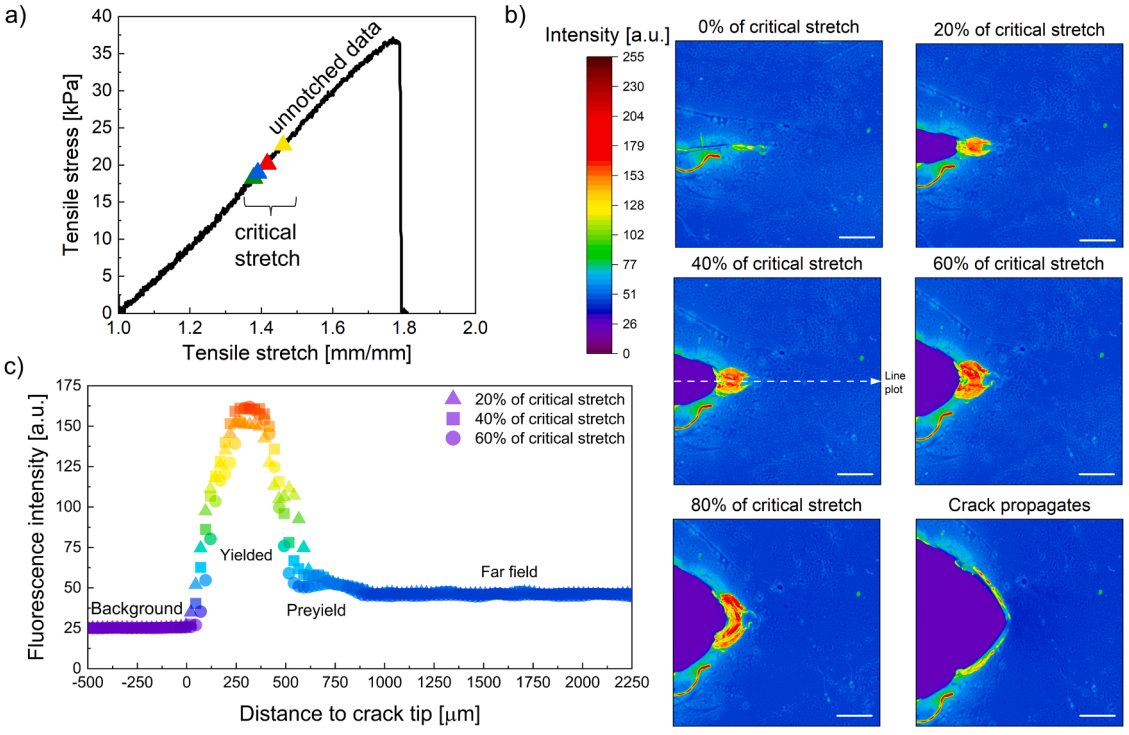

Fig. 7. a) Representative engineering stress-stretch data used for the determination of the critical stretch and fracture toughness values for the 5 wt. % 10 kDa PEG4SH + 1 wt. % alginate DN hydrogel group. b) Representative images of notched mechanochemical experiments for a 5 wt. % 10 kDa PEG4SH + 1 wt. % alginate sample at different stretching levels (scale bar = 500 μm), in which color scale gives the fluorescence intensity in arbitrary units as "a.u." in the figure. c) The fluorescence intensity along the centerline of the image for the three stretching levels (see example line shown in the 40 % critical stretch image). The line profiles were smoothed using Lowess method with raw data exported from ImageJ. The color scale for the fluorescence intensity in the line profiles is identical to the intensity color scale used in b) with arbitrary units as "a.u.".

3.4. Mechanical and mechanochemical response of notched specimens

Results from notched pure shear fracture toughness tests [42,43] using the 5 wt. % 10 kDa PEG4SH + 1 wt. % alginate group are shown in Fig. 7a. When the crack started propagation, the average critical stretch was 1.41 ± 0.03 mm/mm measured from four notched samples and the average fracture toughness was calculated to be $\Gamma_{fracture} = 31.54 \pm 5.31$ J/m^2. While the disulfide linked DN hydrogels fabricated in this study demonstrate improved fracture toughness relative to single network PEG and alginate hydrogels [27,56], the critical stretch and fracture toughness of this DN hydrogel system are lower than reported for other alginate reinforced DN hydrogels [26,27,57] and fracture energies up to ~1000 J/m^2 have been reported for some tough DN systems [34,35,58–61]. The relatively lower fracture toughness explains why there were some gripping point failures (Fig. 4e) for these PEG4SH-alginate DN hydrogels compared to those other studies.

Furthermore, the low toughness is likely attributed to the relatively weak disulfide bonds in the PEG4SH network that are easy to fracture compared to the relatively stronger covalent networks that are used as the backbones for most reported double network hydrogels. To confirm this hypothesis, an intense mechanochemical reaction was observed in response to the high strains associated with a notch tip under pure shear fracture testing for the 5 wt. % 10 kDa PEG4SH + 1 wt. % alginate notched samples. The intense disulfide bond rupture around the notch tips is visualized in Fig. 7b by the reaction with the thiol fluorescent probe IV fluorophore. Cutting the notches before each test broke disulfide bonds along the notch surfaces, creating a bright notch profile with relatively higher intensity before each loading experiment at 0 % of critical stretch in Fig. 7b. The brighter region along the notch extended up to ~250 μm from the notch edge into the sample which was attributed to additional disulfide bonds breaking due to the forces induced by the cutting process. During loading, disulfide bond breakage was intensely localized at the notch tip as visualized by the significantly higher fluorescence intensity at 20–80 % of the critical stretch shown in Fig. 7b. While the visualization of strain distributions and network fracture at notch tips of multi-network hydrogels and elastomers has been achieved in the literature [34,35,49,62], it is important to note that the mechanism in this work is entirely different in that it involves small molecule immobilization. In this study, reaction with the thiol fluorescent probe IV fluorophore represents a convenient way to observe and quantify the small molecule immobilization process prior to immobilizing other functional molecules of interest, as will be described below.

The fracture energy, $\Gamma_{fracture}$, of tough DN hydrogels is generally thought to be the sum of the intrinsic fracture energy, Γ_0, for material separation and the dissipated energy, Γ_{diss}, in the process zone around the crack tip, with Γ_{diss} contributing the larger part the fracture toughness [34,35,58]. The dissipated energy, Γ_{diss}, is often further partitioned into a preyield and yielded process zones ahead of the crack. The contour map in Fig. 7b shows the bright fluorescence of the yielded zone where a large fraction of the PEG4SH network is breaking apart and many free thiols are created. To characterize the damage zone to understand the fracture energy contributions for the PEG disulfide-alginate DN gels, line profiles of fluorescence intensity along the crack propagation direction for PEG disulfide-alginate DN gels loaded to 20–60 % of the critical stretch are plotted in Fig. 7c. The line plots showed the size of the yielded damage zone was around 650 μm with much higher intensity compared to the region far away from the crack tip. Furthermore, a much smaller preyield area was detected in the line plots, where the fluorescence intensity was up to ~30 % larger than the plateau value in the far field region. This preyield increase of around 30 % in fluorescence intensity agrees well with the range seen in the mechanochemical tensile tests where yielding did not occur (Fig. 5b). After the crack started to grow, the bright yielded zone converted into new crack surface, whereas the sample around the new crack displayed fluorescence intensity closer to the far field intensity level as shown in the contour map under 100 % of critical stretch (i.e., crack propagation) in Fig. 7b. The size of damage zone that can be sustained at the notch tip in this work is significantly smaller than has been observed for much tougher DN hydrogels reported by Matsuda et al. (i.e., 1500−2000 μm in their work) [34,35], which reflects the lower fracture toughness of PEG4SH-alginate DN gels. Nonetheless, the goal of this work is to create stretch funtionalizable DN hydrogels rather than optimizing for high fracture toughness alone.

3.5. Cell adhesion after stretch functionalization

Previous studies have demonstrated the cytocompatibility of disulfide linked PEG based hydrogels [10], and as such, in this work we focus on demonstrating how stretch activated molecule immobilization can be utilized for directing cell growth. Because the disulfide bonds are particularly susceptible to breakage through applied mechanical forces, revealing thiol species [10,19,63], we sought to determine whether this highly reactive moiety can then be further utilized to functionalize gels with biologically active motifs. To demonstrate one potential application of the mechanochemically active disulfide linked DN hydrogels, 5 wt. % 10 kDa PEG4SH + 1 wt. % alginate samples, which showed the largest mechanochemical response during tensile testing, were selected for peptide immobilization and cell adhesion experiments. A maleimide containing Gly-Arg-Gly-Asp-Ser peptide (Mal-GRGDS, see Section 2.6.1) was used to react with free thiols formed by disulfide cleavage. The Arg-Gly-Asp (RGD) sequence is a heavily employed cell adhesion motif derived from fibronectin, an adhesive protein inherent in many native extracellular matrices [64]. Since PEG based hydrogels cannot provide the conditions to support cell adhesion due to the absence of active groups for cell-surface interaction [65,66], the maleimide containing RGD peptide (Mal-GRGDS) that would react readily with the free thiol in a Michael-type addition was used to support the seeding of HFF-1 cells on the DN hydrogels, thereby promoting stretch-induced cell attachment points.

Three samples had their surfaces exposed to Mal-GRGDS while they were stretched and held at 75 % of the expected failure strain, while three unstretched samples were exposed to Mal-GRGDS for comparison. Cell adhesion was compared for stretched and unstretched samples. Representative confocal images of human fibroblast (HFF-1) cells seeded on surfaces of unstretched and stretched samples are shown in Figs. 8a and 8b, respectively, indicating approximately 2-fold increase in the number of adherent HFF-1 cells after stretch-induced mechanochemical coupling of Mal-GRGDS (Fig. 8c). This enhanced cell proliferation occurred despite the stretched hydrogel having reduced stiffness relative to the unstretched hydrogel (Fig. 6a), a factor which is well known to decrease cell activity [67]. Cells that attached to the surface showed similar cell spread area for the stretched gels compared to the control group (Fig. 8d).

Hydrogels that were exposed to the Mal-GRGDS peptide while being stretched showed a higher number of attached cells, demonstrating mechanochemical immobilization of the adhesion sequence (Figs. 8a and 8b). It was expected that the stretched gels would have more reactive sites, resulting in a higher degree of functionalization with Mal-GRGDS and therefore greater adhesion of HFF-1 cells as indicated by the significantly higher nuclei count shown in Fig. 8c. However, no impact on cell spreading was also observed (Fig. 8d). This is attributed to the simplicity of the Mal-GRGDS peptide utilized in this study which presents only a single adhesive cue to cells rather than providing multiple adhesive motifs and sequences to facilitate both cellular adhesion and spreading. Future work may focus on tagging full length proteins with maleimide functionality to provide additional bioactivity after stretch-induced mechanochemical activation. Furthermore, the multi-funtionalizable nature of this DN hydrogel system provides scope for force mediated conjugation of various adhesion proteins and growth factors. For example, the mechanochemical responsiveness of the disulfide linkages could be used to enable the binding of adhesion peptides like the RGD motif to effectively promote the local migration and

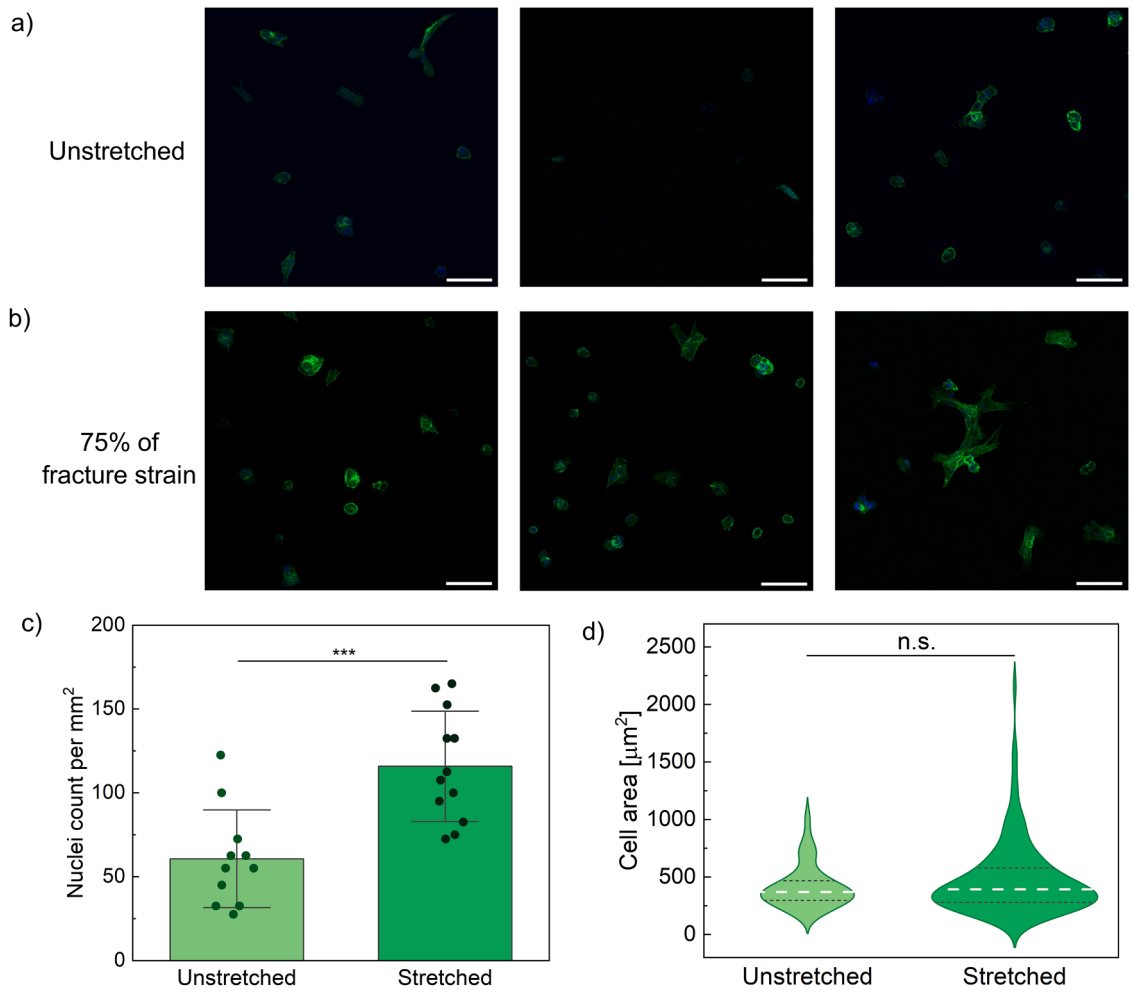

Fig. 8. Representative confocal images of HFF-1 cells seeded on surfaces of 5 wt. % 10 kDa PEG4SH + 1 wt. % alginate DN gels exposed to Mal-GRGDS (scale bar = 100 μm) where a) shows the unstretched samples as the control group and b) shows the hydrogel samples that were exposed to Mal- GRGDS while they were held at 75 % of the fracture strain. Quantitative results of the cell culture experiment showing c) the nuclei count of HFF-1 cells per unit area of hydrogel cell seeding surface ("***" represents $p < 0.001$ in an unpaired *t*-test with Welch's correction) and d) the quantification of cell spreading area of HFF-1 cells ("n.s." represents $p > 0.05$).

proliferation of numerous cell types, which can further enhance biomaterial integration and reduce the risk of rejection [68–70]. Additionally, disulfide-based conjugation with bioactive molecular species and pharmaceutical compounds holds scope for site-specific drug delivery, with potential for applications in force-triggered local therapy for healing and regeneration [14,71,72].

4. Conclusions

The present study provides a first demonstration of how stretch activated small molecule conjugation in tough, disulfide linked polyethylene glycol (PEG4SH) double network (DN) hydrogels reinforced by sodium alginate can be used to functionalize a DN hydrogel in multiple ways. Reinforcement by the alginate network improves the mechanical properties of the PEG4SH network but also shields the disulfide bonds from the applied force to reduce the mechanochemical reaction activation. Thus, there is a need to carefully design DN hydrogels to balance the desired mechanical properties with mechanochemical responsiveness. In this regard, high mechanochemical responsiveness of DN hydrogels under stretching is achieved by relatively low modulus gels that give combinations of high stretch at low stress. An increase in fluorescence intensity during cyclic loading demonstrated disulfide bonds can continue reacting with the local chemical environment during the first force release, while the mechanochemical reaction activation is diminished for the second loading, and negligible for the second unloading. Intense disulfide bond breakage and mechanochemical reaction were observed within the yielded reaction zone of a notch tip which was surrounded by a smaller preyield reaction zone. The disulfide linked PEG4SH-alginate DN hydrogels can also be stretch functionalized to reveal thiol groups for nucleophilic attack of complementary moieties, which is demonstrated by more HFF-1 cells preferentially adhered to DN hydrogels stretched in the presence of a maleimide containing RGD peptide. Together, the findings of this study are anticipated to encourage further research into the development of mechanically stretchable and mechanoresponsive hydrogels that can be mechanochemically functionalized in multiple ways (e.g., for cell culture, tissue engineering, chemosensors, soft robotics, etc.).

CRediT authorship contribution statement

Yuwan Huang: Writing – review & editing, Writing – original draft, Visualization, Methodology, Investigation, Formal analysis. **Zihao Li:** Writing – review & editing, Methodology, Investigation. **Chavinya D. Ranaweera:** Writing – review & editing, Methodology, Investigation. **Pavithra B. Jayathilaka:** Writing – review & editing, Methodology, Investigation. **Md Shariful Islam:** Writing – review & editing, Methodology, Investigation. **Alaa Ajam:** Writing – review & editing, Methodology, Investigation. **Meredith N. Silberstein:** Writing – review & editing, Methodology, Funding acquisition, Formal analysis. **Kristopher A. Kilian:** Writing – review & editing, Supervision, Project

administration, Methodology, Funding acquisition, Conceptualization. **Jamie J. Kruzic:** Writing – review & editing, Writing – original draft, Supervision, Project administration, Methodology, Funding acquisition, Formal analysis, Conceptualization.

Declaration of competing interest

The authors declare that they have no known competing financial interests or personal relationships that could have appeared to influence the work reported in this paper.

Acknowledgements

The authors greatly acknowledge the facilities provided by the Mark Wainwright Analytical Centre at the University of New South Wales. Financial support was provided by the Australian Research Council grants FT180100417 and DP210103654 and by the United States National Air Force Office of Scientific Research under Contract No FA9550-22-1-0030.

Supplementary materials

Supplementary material associated with this article can be found, in the online version, at doi:10.1016/j.actbio.2025.04.013.

References

[1] J. Houk, R. Singh, G.M. Whitesides, Measurement of thiol disulfide interchange reactions and thiol pKa values, Methods Enzymol. 143 (1987) 129–140.
[2] J. Wolff, The classic: on the inner architecture of bones and its importance for bone growth, Clin. Orthop. Relat. R 468 (4) (2010) 1056–1065.
[3] L.C. Palmer, C.J. Newcomb, S.R. Kaltz, E.D. Spoerke, S.I. Stupp, Biomimetic systems for hydroxyapatite mineralization inspired by bone and enamel, Chem. Rev. 108 (11) (2008) 4754–4783.
[4] A. Shaub, Unravelling the extracellular matrix, Nat. Cell Biol. 1 (7) (1999) E173–E175.
[5] A.L. Black, J.M. Lenhardt, S.L. Craig, From molecular mechanochemistry to stress-responsive materials, J. Mater. Chem. 21 (6) (2011) 1655–1663.
[6] M.A. Ghanem, A. Basu, R. Behrou, N. Boechler, A.J. Boydston, S.L. Craig, Y. Lin, B. E. Lynde, A. Nelson, H. Shen, D.W. Storti, The role of polymer mechanochemistry in responsive materials and additive manufacturing, Nat. Rev. Mater. 6 (1) (2021) 84–98.
[7] G. Kaupp, Mechanochemistry: the varied applications of mechanical bond-breaking, Cryst. Eng. Comm. 11 (3) (2009) 388–403.
[8] A.A. Dombkowski, K.Z. Sultana, D.B. Craig, Protein disulfide engineering, FEBS Lett. 588 (2) (2014) 206–212.
[9] S. Bian, M. He, J. Sui, H. Cai, Y. Sun, J. Liang, Y. Fan, X. Zhang, The self-crosslinking smart hyaluronic acid hydrogels as injectable three-dimensional scaffolds for cells culture, Colloids Surf. B-Biointerf. 140 (2016) 392–402.
[10] J. Lee, M.N. Silberstein, A.A. Abdeen, S.Y. Kim, K.A. Kilian, Mechanochemical functionalization of disulfide linked hydrogels, Mater. Horiz. 3 (5) (2016) 447–451.
[11] X.Z. Shu, Y. Liu, F. Palumbo, G.D. Prestwich, Disulfide-crosslinked hyaluronan-gelatin hydrogel films: a covalent mimic of the extracellular matrix for in vitro cell growth, Biomaterials 24 (21) (2003) 3825–3834.
[12] K. Yamauchi, N. Takeuchi, A. Kurimoto, T. Tanabe, Films of collagen crosslinked by S-S bonds: preparation and characterization, Biomaterials 22 (8) (2001) 855–863.
[13] M.H. Lee, J.L. Sessler, J.S. Kim, Disulfide-based multifunctional conjugates for targeted theranostic drug delivery, Accounts Chem. Res. 48 (11) (2015) 2935–2946.
[14] D. Yang, W. Chen, J. Hu, Design of controlled drug delivery system based on disulfide cleavage trigger, J. Phys. Chem. B 118 (43) (2014) 12311–12317.
[15] C. Yang, M. Wang, H. Haider, J. Yang, J.-Y. Sun, Y. Chen, J. Zhou, Z. Suo, Strengthening alginate/polyacrylamide hydrogels using various multivalent cations, ACS Appl. Mater. Inter. 5 (24) (2013) 10418–10422.
[16] M. Gajendiran, J.S. Rhee, K. Kim, Recent developments in thiolated polymeric hydrogels for tissue engineering applications, Tissue Eng. Pt B Rev. 24 (1) (2018) 66–74.
[17] S.-W. Wu, X. Liu, A.L. Miller II, Y.-S. Cheng, M.-L. Yeh, L. Lu, Strengthening injectable thermo-sensitive NIPAAm-g-chitosan hydrogels using chemical cross-linking of disulfide bonds as scaffolds for tissue engineering, Carbohydr. Polym. 192 (2018) 308–316.
[18] G. Deng, F. Li, H. Yu, F. Liu, C. Liu, W. Sun, H. Jiang, Y. Chen, Dynamic hydrogels with an environmental adaptive self-healing ability and dual responsive sol-gel transitions, ACS. Macro Lett. 1 (2) (2012) 275–279.
[19] K.R. Fitch, A.P. Goodwin, Mechanochemical reaction cascade for sensitive detection of covalent bond breakage in hydrogels, Chem. Mater. 26 (23) (2014) 6771–6776.
[20] H. Yu, Y. Wang, H. Yang, K. Peng, X. Zhang, Injectable self-healing hydrogels formed via thiol/disulfide exchange of thiol functionalized F127 and dithiolane modified PEG, J. Mater. Chem. B 5 (22) (2017) 4121–4127.
[21] L.M. Saiz, M.G. Prolongo, V. Bonache, A. Jimenez-Suarez, S.G. Prolongo, Self-healing materials based on disulfide bond-containing acrylate networks, Polym. Test. 117 (2023) 107832.
[22] V.T. Tran, M.T.I. Mredha, J.Y. Na, J.-K. Seon, J. Cui, I. Jeon, Multifunctional poly (disulfide) hydrogels with extremely fast self-healing ability and degradability, Chem. Eng. Sci. 394 (2020) 124941.
[23] P. Casuso, I. Odriozola, A. Pérez-San Vicente, I. Loinaz, G. Cabañero, H.-J. Grande, D. Dupin, Injectable and self-healing dynamic hydrogels based on metal(I)-thiolate/disulfide exchange as biomaterials with tunable mechanical properties, Biomacromolecules 16 (11) (2015) 3552–3561.
[24] A.V. Parameswar, K.R. Fitch, D.S. Bull, V.R. Duke, A.P. Goodwin, Polyacrylamide hydrogels produce hydrogen peroxide from osmotic swelling in aqueous media, Biomacromolecules 19 (8) (2018) 3421–3426.
[25] M.M. Perera, D.M. Fischesser, J.D. Molkentin, N. Ayres, Stiffness of thermoresponsive gelatin-based dynamic hydrogels affects fibroblast activation, Polym. Chem. 10 (46) (2019) 6360–6367.
[26] S. Hong, D. Sycks, H.F. Chan, S. Lin, G.P. Lopez, F. Guilak, K.W. Leong, X. Zhao, 3D printing of highly stretchable and tough hydrogels into complex, cellularized structures, Adv. Mater. 27 (27) (2015) 4035–4040.
[27] J.-Y. Sun, X. Zhao, W.R.K. Illeperuma, O. Chaudhuri, K.H. Oh, D.J. Mooney, J. J. Vlassak, Z. Suo, Highly stretchable and tough hydrogels, Nature 489 (7414) (2012) 133–136.
[28] Y. Huang, P.B. Jayathilaka, M.S. Islam, C.B. Tanaka, M.N. Silberstein, K.A. Kilian, J.J. Kruzic, Structural aspects controlling the mechanical and biological properties of tough, double network hydrogels, Acta Biomater. 138 (2022) 301–312.
[29] H. Chen, F. Yang, Q. Chen, J. Zheng, A novel design of multi-mechanoresponsive and mechanically strong hydrogels, Adv. Mater. 29 (21) (2017) 1606900.
[30] B. Xu, Z. Luo, R. Xiao, Z. Wang, J. Yang, Hybrid phenol-rhodamine dye based mechanochromic double network hydrogels with tunable stress sensitivity, Macromol. Rapid Comm. 43 (23) (2022) 2200580.
[31] B. Xu, H. Wang, Z. Luo, J. Yang, Z. Wang, Multi-material 3D printing of mechanochromic double network hydrogels for on-demand patterning, ACS Appl. Mater. Inter. 15 (8) (2023) 11122–11130.
[32] F. Yang, X. Li, Y. Chen, A chromic and near-infrared emissive mechanophore serving as a versatile force meter in micelle-hydrogel composites, Adv. Opt. Mater. 10 (9) (2022) 2102552.
[33] Y. Yuan, H. Zhang, J. Qu, Pyridine-dicarbohydrazone-based polyacrylate hydrogels with strong mechanical property, tunable/force-induced fluorescence, and thermal/ph stimuli responsiveness, ACS. Appl. Polym. Mater. 3 (9) (2021) 4512–4522.
[34] T. Matsuda, R. Kawakami, T. Nakajima, J.P. Gong, Crack tip field of a double-network gel: visualization of covalent bond scission through mechanoradical polymerization, Macromolecules. 53 (20) (2020) 8787–8795.
[35] T. Matsuda, R. Kawakami, T. Nakajima, Y. Hane, J.P. Gong, Revisiting the origins of the fracture energy of tough double-network hydrogels with quantitative mechanochemical characterization of the damage zone, Macromolecules. 54 (22) (2021) 10331–10339.
[36] K. Fang, R. Wang, H. Zhang, L. Zhou, T. Xu, Y. Xiao, Y. Zhou, G. Gao, J. Chen, D. Liu, F. Ai, J. Fu, Mechano-responsive, tough, and antibacterial zwitterionic hydrogels with controllable drug release for wound healing applications, ACS Appl. Mater. Inter. 12 (47) (2020) 52307–52318.
[37] P.B. Jayathilaka, T.G. Molley, Y. Huang, M.S. Islam, M.R. Buche, M.N. Silberstein, J.J. Kruzic, K.A. Kilian, Force-mediated molecule release from double network hydrogels, Chem. Commun. 57 (68) (2021) 8484–8487.
[38] T. Matsuda, R. Kawakami, R. Namba, T. Nakajima, J.P. Gong, Mechanoresponsive self-growing hydrogels inspired by muscle training, Science 363 (6426) (2019) 504–508.
[39] M. Liu, J. Guo, C.Y. Hui, A.T. Zehnder, Application of digital image correlation (DIC) to the measurement of strain concentration of a pva dual-crosslink hydrogel under large deformation, Exp. Mech. 59 (2019) 1021–1032.
[40] Y. Mao, S. Lin, X. Zhao, L. Anand, A large deformation viscoelastic model for double-network hydrogels, J. Mech. Phys. Solids. 100 (2017) 103–130.
[41] R.K.A. Pasumarthy, H.V. Tippur, Mechanical and optical characterization of a tissue surrogate polymer gel, Polym. Test. 55 (2016) 219–229.
[42] R. Long, C.-Y. Hui, Fracture toughness of hydrogels: measurement and interpretation, Soft. Matter. 12 (39) (2016) 8069–8086.
[43] R.S. Rivlin, A.G. Thomas, Rupture of rubber. I. Characteristic energy for tearing, J. Polym. Sci. 10 (3) (1953) 291–318.
[44] E.M. Arruda, M.C. Boyce, A three-dimensional constitutive model for the large stretch behavior of rubber elastic materials, J. Mech. Phys. Solids. 41 (2) (1993) 389–412.
[45] M.C. Boyce, E.M. Arruda, Swelling and mechanical stretching of elastomeric materials, Math. Mech. Solids. 6 (6) (2001) 641–659.
[46] C. Baumann, M. Stratigaki, S.P. Centeno, R. Gostl, Multicolor mechanofluorophores for the quantitative detection of covalent bond scission in polymers, Angew. Chem. Int. Ed. 60 (24) (2021) 13287–13293.
[47] J.M. Clough, C. Creton, S.L. Craig, R.P. Sijbesma, Covalent bond scission in the mullins effect of a filled elastomer: real-time visualization with mechanoluminescence, Adv. Funct. Mater. 26 (48) (2016) 9063–9074.

[48] D.A. Davis, A. Hamilton, J. Yang, L.D. Cremar, D. Van Gough, S.L. Potisek, M. T. Ong, P.V. Braun, T.J. Martinez, S.R. White, J.S. Moore, N.R. Sottos, Force-induced activation of covalent bonds in mechanoresponsive polymeric materials, Nature 459 (7243) (2009) 68–72.
[49] E. Ducrot, Y. Chen, M. Bulters, R.P. Sijbesma, C. Creton, Toughening elastomers with sacrificial bonds and watching them break, Science 344 (6180) (2014) 186–189.
[50] M. Stratigaki, C. Baumann, L.C.A. van Breemen, J.P.A. Heuts, R.P. Sijbesma, R. Göstl, Fractography of poly(N-isopropylacrylamide) hydrogel networks crosslinked with mechanofluorophores using confocal laser scanning microscopy, Polym. Chem. 11 (2) (2020) 358–366.
[51] L. Yi, H. Li, L. Sun, L. Liu, C. Zhang, Z. Xi, A highly sensitive fluorescence probe for fast thiol-quantification assay of glutathione reductase, Angewandte Chemie Int. Ed. 48 (22) (2009) 4034–4037.
[52] V. Borsenberger, M. Kukwikila, S. Howorka, Synthesis and enzymatic incorporation of modified deoxyuridine triphosphates, Org. Biomol. Chem. 7 (18) (2009) 3826–3835.
[53] A. Ajam, Y. Huang, M.S. Islam, K.A. Kilian, J.J. Kruzic, Mechanical and biological behavior of double network hydrogels reinforced with alginate versus gellan gum, J. Mech. Behav. Biomed. Mater. 157 (2024) 106642.
[54] Z. Jing, X. Dai, X. Xian, X. Du, M. Liao, P. Hong, Y. Li, Tough, stretchable and compressive alginate-based hydrogels achieved by non-covalent interactions, RSC. Adv. 10 (40) (2020) 23592–23606.
[55] Z. Zhang, T. Lin, S. Li, X. Chen, X. Que, L. Sheng, Y. Hu, J. Peng, H. Ma, J. Li, W. Zhang, M. Zhai, Polyacrylamide/copper-alginate double network hydrogel electrolyte with excellent mechanical properties and strain-sensitivity, Macromol. Biosci. 22 (2) (2022) 2100361.
[56] S. Lin, J. Ni, D. Zheng, X. Zhao, Fracture and fatigue of ideal polymer networks, Extreme Mech. Lett. 48 (2021) 101399.
[57] J. Li, W.B.K. Illeperuma, Z. Suo, J.J. Vlassak, Hybrid hydrogels with extremely high stiffness and toughness, ACS. Macro Lett. 3 (6) (2014) 520–523.
[58] Y. Jia, Z. Zhou, H. Jiang, Z. Liu, Characterization of fracture toughness and damage zone of double network hydrogels, J. Mech. Phys. Solids. 169 (2022) 105090.
[59] T. Nakajima, H. Furukawa, Y. Tanaka, T. Kurokawa, J.P. Gong, Effect of void structure on the toughness of double network hydrogels, J. Polym. Sci. Pol. Phys. 49 (17) (2011) 1246–1254.
[60] H. Xin, S.Z. Saricilar, H.R. Brown, P.G. Whitten, G.M. Spinks, Effect of first network topology on the toughness of double network hydrogels, Macromolecules. 46 (16) (2013) 6613–6620.
[61] Y. Yang, X. Wang, F. Yang, H. Shen, D. Wu, A universal soaking strategy to convert composite hydrogels into extremely tough and rapidly recoverable double-network hydrogels, Adv. Mater. 28 (33) (2016) 7178–7184.
[62] Y. Zheng, Y. Wang, T. Nakajima, J.P. Gong, Effect of predamage on the fracture energy of double-network hydrogels, ACS. Macro Lett. 13 (2) (2024) 130–137.
[63] A.E.M. Beedle, M. Mora, C.T. Davis, A.P. Snijders, G. Stirnemann, S. Garcia-Manyes, Forcing the reversibility of a mechanochemical reaction, Nat. Commun. 9 (2018) 3155.
[64] M.D. Pierschbacher, E. Ruoslahti, Cell attachment activity of fibronectin can be duplicated by small synthetic fragments of the molecule, Nature 309 (5963) (1984) 30–33.
[65] J.M. Zhu, Bioactive modification of poly(ethylene glycol) hydrogels for tissue engineering, Biomaterials 31 (17) (2010) 4639–4656.
[66] P. Lu, D. Ruan, M. Huang, M. Tian, K. Zhu, Z. Gan, Z. Xiao, Harnessing the potential of hydrogels for advanced therapeutic applications: current achievements and future directions, Signal Transduct. Tar. 9 (1) (2024) 166.
[67] D.E. Discher, P. Janmey, Y.-l. Wang, Tissue cells feel and respond to the stiffness of their substrate, Science 310 (5751) (2005) 1139–1143.
[68] S.L. Bellis, Advantages of RGD peptides for directing cell association with biomaterials, Biomaterials 32 (18) (2011) 4205–4210.
[69] D. Missirlis, J.P. Spatz, Combined effects of PEG hydrogel elasticity and cell-adhesive coating on fibroblast adhesion and persistent migration, Biomacromolecules 15 (1) (2014) 195–205.
[70] R. Rangel, W.B. Swanson, D.T. Wu, The future of cell-instructive biomaterials for tissue regeneration-a perspective from early career clinician-scientists, Front. Mater. 10 (2024) 1328904.
[71] M.H. Lee, Z. Yang, C.W. Lim, Y.H. Lee, S. Dongbang, C. Kang, J.S. Kim, Disulfide-cleavage-triggered chemosensors and their biological applications, Chem. Rev. 113 (7) (2013) 5071–5109.
[72] M. Danial, A. Postma, Disulfide conjugation chemistry: a mixed blessing for therapeutic drug delivery? Ther. Deliv. 8 (6) (2017) 359–362.